INSTITUTE OF PHYSICS PUBLISHING JOURNAL OF PHYSICS B: ATOMIC, MOLECULAR AND OPTICAL PHYSICS

J. Phys. B: At. Mol. Opt. Phys. **34** (2001) L457–L466 PII: S0953-4075(01)23877-2

LETTER TO THE EDITOR

Fully quantal (γ, 2e) calculations for absolute differential cross sections of helium

J Colgan, M S Pindzola and F Robicheaux

Department of Physics, Auburn University, Auburn, AL 36849, USA

Received 5 April 2001, in final form 11 June 2001
Published 13 July 2001
Online at stacks.iop.org/JPhysB/34/L457

Abstract

The formulation of the time-dependent close-coupling method is extended so that energy and angle differential cross sections for the double photoionization of helium may be obtained. The fully quantal method now yields absolute total integral, energy differential, and angle differential cross sections. A detailed comparison is made with the absolute synchrotron measurements of Bräuning *et al* (1998 *J. Phys. B: At. Mol. Opt. Phys.* **31** 5149–60) for triple differential cross sections at 20 eV excess photon energy. The agreement between theory and experiment is excellent.

An accurate description of the continuum state of three interacting charged particles remains the key ingredient in the calculation of absolute integral and differential cross sections for the double photoionization of helium. In the absence of an analytical solution and encouraged by the spectacular power of modern computing platforms, direct numerical approaches to the calculation of the correlated double continuum wavefunction have been made in recent years. Integral and differential cross sections for the double photoionization of helium have been calculated using the double screened Coulomb [1,2], the converged close-coupling [3,4] and the hyperspherical R-matrix [5, 6] methods. The even more challenging integral and differential cross sections for the electron-impact ionization of hydrogen have been calculated using the exterior complex scaling [7] and the converged close-coupling [8,9] methods. In both ionization processes, the most demanding test for the theoretical methods has been comparison with experimental measurements [10–12] of absolute triple differential cross sections. Each numerical approach, with it's particular balance of strengths and weaknesses, provides new insight into the treatment and understanding of the long range dynamics of three interacting charged particles.

In this letter we extend the time-dependent close-coupling method to the calculation of absolute energy and angle differential cross sections for the double photoionization of helium. Previous work [13] on total integral cross sections yielded ratios of double photoionization to single photoionization that are in good agreement with experimental measurements [14–16] from threshold to 200 eV incident photon energy. For ejected-energy differential cross sections, we project the time-dependent two-dimensional radial wavefunction onto product states of Coulomb continuum radial orbitals and then sum the resulting momentum space amplitudes

incoherently. Using many more partial waves, the same method has been used successfully to obtain ejected-energy differential cross sections for the electron-impact ionization of helium [17] and lithium [18]. For ejected-energy and angle differential cross sections, the key step is to weight the momentum space amplitudes by coupled momentum spherical harmonics and then sum coherently. We remark here that the outgoing flux is not computed due to problems that would be encountered near the box boundary due to single ionization. After a brief summary of the working equations (atomic units are used throughout this letter), we compare the time-dependent close-coupling results with the absolute synchrotron measurements of Bräuning *et al* [10] for triple differential cross sections of helium at 20 eV excess photon energy.

The ground state of helium is found by relaxation of the time-dependent Schrödinger equation in imaginary time ($\tau = it$):

$$\frac{-\partial \Phi_0^{1\mathrm{S}}(\vec{r}_1, \vec{r}_2, \tau)}{\partial \tau} = H_{\mathrm{atom}} \Phi_0^{1\mathrm{S}}(\vec{r}_1, \vec{r}_2, \tau) \tag{1}$$

where the non-relativistic Hamiltonian is given by:

$$H_{\mathrm{atom}} = -\frac{1}{2}\nabla_1^2 - \frac{1}{2}\nabla_2^2 - \frac{Z}{r_1} - \frac{Z}{r_2} + \frac{1}{|\vec{r}_1 - \vec{r}_2|} \tag{2}$$

with $Z = 2$ for helium. The six-dimensional ground state wavefunction is expanded in coupled spherical harmonics:

$$\Phi_0^{1\mathrm{S}}(\vec{r}_1, \vec{r}_2, \tau) = \sum_{l=0}^{l_0} \frac{P_{ll}^{1\mathrm{S}}(r_1, r_2, \tau)}{r_1 r_2} Y_{ll}^{1\mathrm{S}}(\hat{r}_1, \hat{r}_2) \tag{3}$$

where $l_0 = 3$ is sufficient for convergence. Substituting equations (2) and (3) into equation (1) yields a set of coupled partial differential equations for the two-dimensional radial wavefunctions, $P_{ll}^{1\mathrm{S}}(r_1, r_2, \tau)$, that may be solved on a numerical lattice using standard finite difference methods [13]. About 500 imaginary time steps at $\Delta\tau = 0.01$ are needed to achieve convergence on a uniform lattice with a mesh spacing of $\Delta r = 0.1$ if one begins with $P_{ll}^{1\mathrm{S}}(r_1, r_2, \tau = 0) = \delta_{l,0} P_{1\mathrm{s}}(r_1) P_{1\mathrm{s}}(r_2)$, where $P_{1\mathrm{s}}(r)$ is a bound state radial orbital for He^+. The correlated ground state wavefunction for helium has a total energy of $E_0 = -78.1$ eV on the lattice. Further improvements in the absolute value of the total energy (chemical accuracy is -79.0 eV) could be achieved by an even smaller mesh spacing (see [13] for further discussion), or by use of a non-uniform mesh. We remark that the uniform mesh is ideal for the current calculation of double ionization processes, where the treatment of the continuum is the crucial factor. Of course highly sophisticated bound state methods exist which calculate the ground state energy of helium to many decimal places in accuracy, but may not be suitable for representing the continuum.

We now solve the 'weak field' time-dependent Schrödinger equation in real time:

$$\mathrm{i}\frac{\partial \Psi^{1\mathrm{P}}(\vec{r}_1, \vec{r}_2, t)}{\partial t} = H_{\mathrm{atom}} \Psi^{1\mathrm{P}}(\vec{r}_1, \vec{r}_2, t) + H_{\mathrm{rad}} \Phi_0^{1\mathrm{S}}(\vec{r}_1, \vec{r}_2, \tau = \infty) \mathrm{e}^{-\mathrm{i}E_0 t} \tag{4}$$

where the Hamiltonian for a linearly polarized radiation field in the length gauge is given by:

$$H_{\mathrm{rad}} = E(t)(r_1 \cos\theta_1 + r_2 \cos\theta_2) \cos\omega t \tag{5}$$

with electric field amplitude $E(t)$ and radiation frequency ω. The electric field is ramped on smoothly over one quarter of a field period so that $E(t) = t/T$ for $t < T/4$, $E(t) = 1$ for $t > T/4$. The velocity gauge may also be used, but previous time-dependent close-coupling calculations [13] for the double photoionization cross sections of helium have been found to

be gauge invariant. The six-dimensional photoabsorption state wavefunction is also expanded in coupled spherical harmonics:

$$\Psi^{^1\mathrm{P}}(\vec{r}_1, \vec{r}_2, t) = \sum_{l_1,l_2} \frac{P^{^1\mathrm{P}}_{l_1 l_2}(r_1, r_2, t)}{r_1 r_2} Y^{^1P}_{l_1 l_2}(\hat{r}_1, \hat{r}_2) \tag{6}$$

where $l_1 \leqslant 3$ and $l_2 \leqslant 3$ is sufficient. Substituting equations (2), (3), (5), and (6) into equation (4) yields a set of coupled partial differential equations for the two-dimensional radial wavefunctions, $P^{^1\mathrm{P}}_{l_1 l_2}(r_1, r_2, t)$, that may also be solved on a numerical lattice [13]. Keeping the same mesh spacing of $\Delta r = 0.1$ and beginning with $P^{^1\mathrm{P}}_{l_1 l_2}(r_1, r_2, t = 0) = 0$ for all l_1, l_2, the close-coupled equations are time propagated for between 10 and 15 radiation field periods ($\frac{2\pi}{\omega}$). A lattice size of 600×600 points is employed. Increasing the lattice to 1000×1000 points made a difference of no more than 2% in the results presented in this letter. The wavefunction defined in equation (6) is initially anti-symmetrized as discussed previously [13], and will remain so under time propagation. We note also that the radial wavefunctions $P^{^1\mathrm{P}}_{l_1 l_2}(r_1, r_2, t)$ are symmetric under interchange of r_1 and r_2.

The total photoabsorption probability is given by:

$$\mathcal{P} = \sum_{l_1,l_2} \int_0^\infty \mathrm{d}r_1 \int_0^\infty \mathrm{d}r_2 |P^{^1\mathrm{P}}_{l_1 l_2}(r_1, r_2, t)|^2. \tag{7}$$

Using standard projection techniques onto symmetrized products of distorted continuum waves, the total double photoionization probability is given by:

$$\mathcal{P}_{\mathrm{dion}} = \sum_{l_1,l_2} \int_0^\infty \mathrm{d}k_1 \int_0^\infty \mathrm{d}k_2 |P^{^1\mathrm{P}}_{l_1 l_2}(k_1, k_2, t)|^2 \tag{8}$$

where

$$P^{^1\mathrm{P}}_{l_1 l_2}(k_1, k_2, t) = \int_0^\infty \mathrm{d}r_1 \int_0^\infty \mathrm{d}r_2 P_{k_1 l_1}(r_1) P_{k_2 l_2}(r_2) P^{^1\mathrm{P}}_{l_1 l_2}(r_1, r_2, t) \tag{9}$$

and $P_{kl}(r)$ is a continuum state radial orbital for He^+. Both total probabilities may be monitored as a function of time. Time propagations have converged when the rate of change of the total double photoionization probability becomes constant. In general, larger lattice sizes and longer propagation times are needed as the excess photon energy, defined by $\Delta E = \omega + E_0$, becomes smaller.

The continuum state radial orbitals found in equation (9) may be obtained by direct diagonalization of the time-independent radial Hamiltonian for He^+:

$$h_{\mathrm{ion}} = -\frac{1}{2}\frac{\mathrm{d}^2}{\mathrm{d}r^2} + \frac{l(l+1)}{2r^2} - \frac{2}{r} \tag{10}$$

on a one-dimensional numerical lattice with a constant mesh spacing of again $\Delta r = 0.1$. The size of the lattice determines the distribution of bound and continuum states. We also note that even for a constant box size, the energy distribution of bound and continuum states changes for each l. We may also obtain the continuum state radial orbitals by direct numerical integration of the time-independent Schrödinger equation for He^+:

$$(h_{\mathrm{ion}} - \tfrac{k^2}{2}) P_{kl}(r) = 0. \tag{11}$$

The standard box normalization is given by:

$$P_{kl}(r) \to \sqrt{\frac{2\Delta k}{\pi}} \sin\left(kr + \frac{q}{k} ln(2kr) - \frac{l\pi}{2} + \delta_l\right) \tag{12}$$

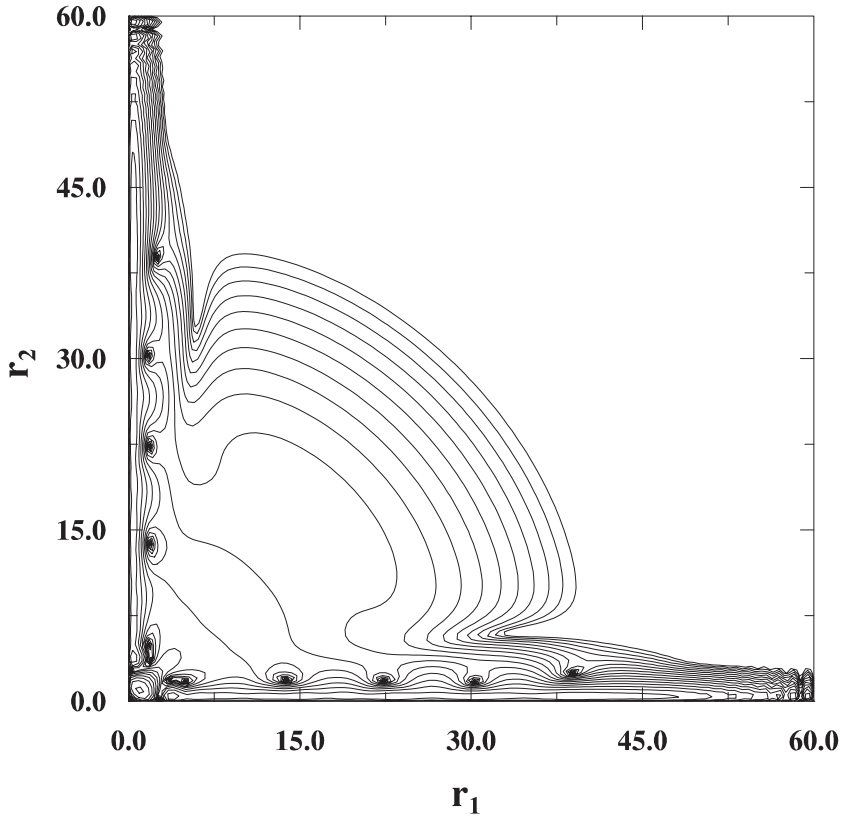

Figure 1. Contour plot of $\sum_{l_1,l_2} |P^{^1\mathrm{P}}_{l_1 l_2}(r_1, r_2, t)|^2$, the total photoabsorption probability density as defined in equation (7), after 15 radiation field periods at 20 eV excess photon energy (r_1 and r_2 are in atomic units).

where Δk is the momentum mesh spacing, $q = 2$ is the asymptotic charge and δ_l is the Coulomb phase shift. Note, that as the density of states increases for smaller Δk mesh spacing, the amplitude of any one continuum wave decreases. We use a total of 600 continuum state radial orbitals on a uniform momentum mesh with $\Delta k = 0.0025$.

In generating the continuum functions by direct integration over a fixed energy (momentum) mesh, with the box normalization defined in equation (12) we ensure that, for all angular momenta, the continuum orbital amplitudes are calculated at the same energy points. This allows us to add the continuum orbital amplitudes coherently, which is necessary in the calculation of angle differential cross sections. We point out here also that we calculated the total double photoionization cross section using both methods of generating continuum orbitals and found excellent agreement between the two methods. This validates our use of the second method described when calculating angle differential cross sections.

For an excess photon energy of 20 eV, we present the total photoabsorption probability density of equation (7) as a function of r_1 and r_2 in figure 1, after a time propagation of 15 radiation field periods. Single photoionization may be identified with the high ridges along each radial axis. A single photoelectron with all 75 eV excess photon energy has time to move out to the edge of the box, and even begin to reflect back. Although an absorbing potential may be used to suppress the reflected waves, it was not deemed necessary in this calculation as the

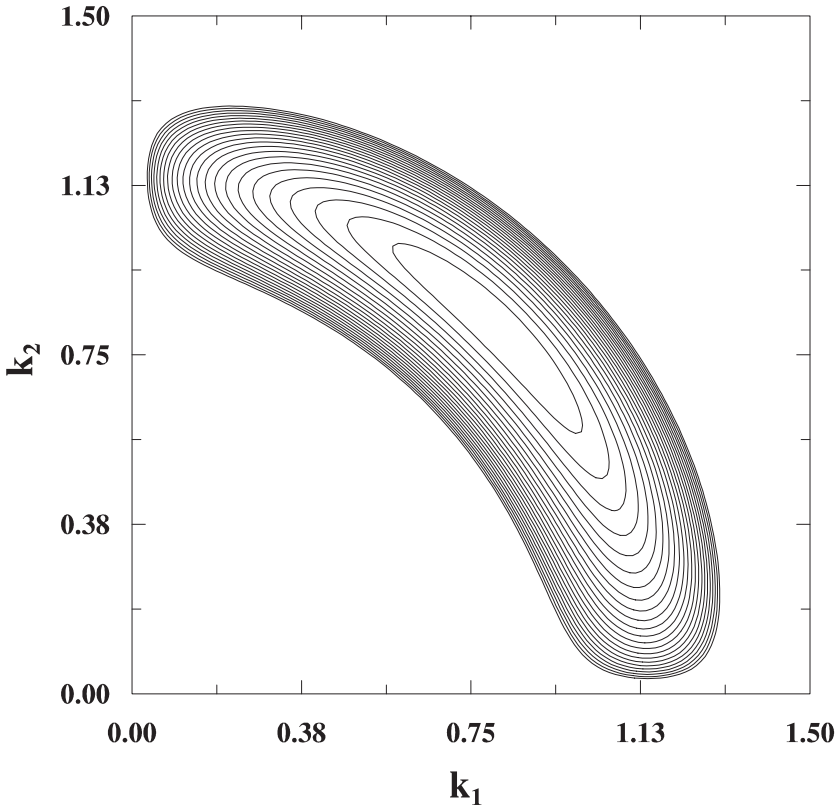

Figure 2. Contour plot of $\sum_{l_1,l_2} |P^{^1\mathrm{P}}_{l_1 l_2}(k_1, k_2, t)|^2$, the total double photoionization probability as defined in equation (8), after 15 radiation field periods at 20 eV excess photon energy (k_1 and k_2 are in atomic units).

reflection back into the double ionization region is negligible. Double photoionization may be identified with the broad plateau on either side of the $r_1 = r_2$ axis. Since the two photoelectrons share the 20 eV, the broad plateau has not journeyed as far in the $r_1 r_2$ plane. For the same excess photon energy, and after the same number of radiation field periods, we present the total double photoionization probability density of equation (8) as a function of k_1 and k_2 in figure 2. The probability peaks at $\alpha = 45^\circ$, where $\tan\alpha = \frac{k_2}{k_1}$ defines the hyperspherical angle. The probability ridge is a quarter of the circle defined by the energy conservation condition

$$\Delta E = \frac{k_1^2}{2} + \frac{k_2^2}{2}.$$

The total integral cross section for double photoionization is given by:

$$\sigma_{\mathrm{dion}} = \frac{\omega}{I}\frac{\partial \mathcal{P}_{\mathrm{dion}}}{\partial t} \tag{13}$$

where I is the radiation field intensity. For an excess photon energy of 20 eV, the time-dependent close-coupling calculation yields a total integral cross section of 8.99 kb, where $1.0\ \mathrm{kb} = 1.0 \times 10^{-21}\ \mathrm{cm}^2$. This agrees well with the experimental result of 8.76 kb found by Samson *et al* [16].

The single differential cross section for double photoionization may be defined in several

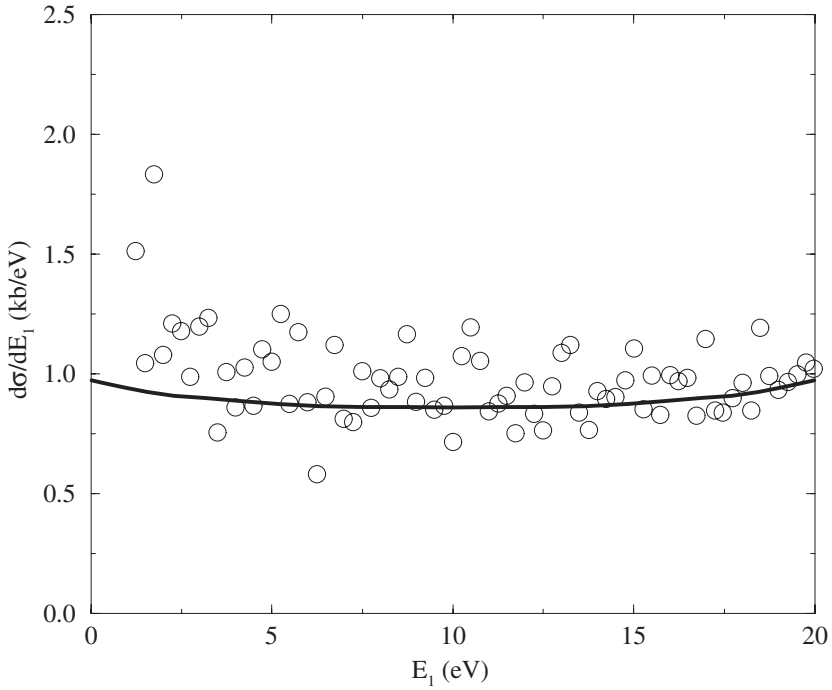

Figure 3. Single energy differential cross section in kb/eV for helium at 20 eV excess photon energy. Full curve: present calculation; open circles: experimental points of Wehlitz *et al* [19]. ($1.0\ \mathrm{kb} = 1.0 \times 10^{-21}\ \mathrm{cm}^2$).

equivalent forms:

$$\sigma_{\mathrm{dion}} = \int_0^{\pi/2} \frac{\mathrm{d}\sigma}{\mathrm{d}\alpha}\mathrm{d}\alpha = \int_0^{\Delta E} \frac{\mathrm{d}\sigma}{\mathrm{d}E_1}\mathrm{d}E_1 = \int_0^{\Delta E/2} \frac{\mathrm{d}\bar{\sigma}}{\mathrm{d}E_1}\mathrm{d}E_1 \tag{14}$$

where $E_1 = \frac{k_1^2}{2}$. The hyperspherical angle differential cross section is given by:

$$\frac{\mathrm{d}\sigma}{\mathrm{d}\alpha} = \frac{\omega}{I}\frac{\partial}{\partial t}\int_0^{\infty}\mathrm{d}k_1\int_0^{\infty}\mathrm{d}k_2\,\delta\left(\alpha - \tan^{-1}\left(\frac{k_2}{k_1}\right)\right)\sum_{l_1,l_2}|P^{^1\mathrm{P}}_{l_1 l_2}(k_1,k_2,t)|^2. \tag{15}$$

Since figure 2 shows $\sum_{l_1,l_2}|P^{^1\mathrm{P}}_{l_1 l_2}(k_1,k_2,t)|^2$ the rate of change of this function will yield the single differential cross section.

The 'natural' ejected-energy differential cross section is given by:

$$\frac{\mathrm{d}\sigma}{\mathrm{d}E_1} = \frac{1}{k_1 k_2}\frac{\mathrm{d}\sigma}{\mathrm{d}\alpha}. \tag{16}$$

The transformation factors in the denominator will reduce the ejected-energy differential cross section near the region where $k_1 = k_2$, whereas the hyperspherical angle differential cross section is at a maximum in this region. Finally, due to the symmetry of the single differential cross section about the $k_1 = k_2$ axis, it has become the convention to define the ejected-energy differential cross section:

$$\frac{\mathrm{d}\bar{\sigma}}{\mathrm{d}E_1} = 2\frac{\mathrm{d}\sigma}{\mathrm{d}E_1}. \tag{17}$$

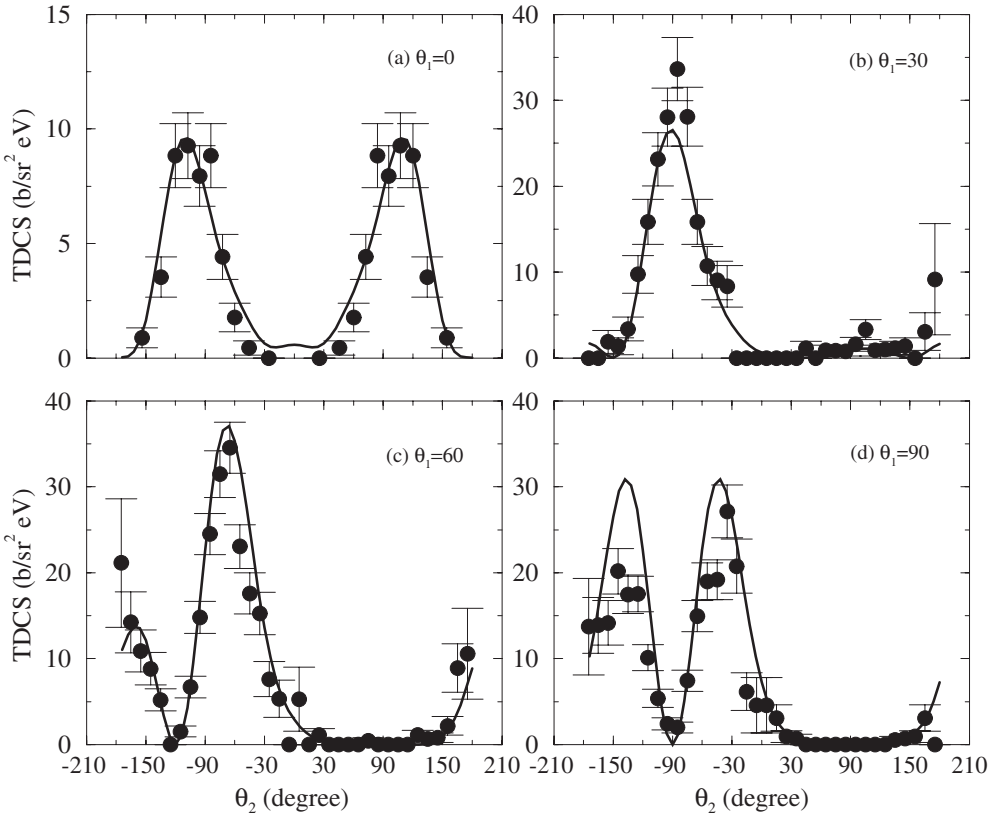

Figure 4. Triple differential cross sections in b/sr^2 eV for helium, as a function of θ_2, the angle of the second ejected electron, for different fixed values of θ_1 as indicated and for equal energy sharing $E_1 = E_2 = 10$ eV between the two ejected electrons. The full curves are the present calculations and the full circles are the absolute experimental measurements of Bräuning *et al* [10]. (1.0b $= 1.0 \times 10^{-24}$ cm^2).

We will stay with the convention. For an excess photon energy of 20 eV, the ejected-energy differential cross section for double photoionization is presented in figure 3. The time-dependent close-coupling results are smooth and quite flat for all values of E_1 from 0 to the maximum value of 20 eV. The experimental measurements of Wehlitz *et al* [19] oscillate about our theoretical results. Remember, that in this convention, the area under the curve from 0 to 10 eV yields the total integral cross section.

The triple differential cross section for double photoionization is defined by:

$$\sigma_{\rm dion} = \int_0^{\pi/2} {\rm d}\alpha \int {\rm d}\Omega_1 \int {\rm d}\Omega_2 \frac{{\rm d}^3\sigma}{{\rm d}\alpha {\rm d}\Omega_1 {\rm d}\Omega_2}. \tag{18}$$

Since for long times following the collision $\vec{r} \rightarrow \vec{k}T$, the differential cross section in the hyperspherical angle and the solid angles for the emission of both photoelectrons is given by:

$$\frac{{\rm d}^3\sigma}{{\rm d}\alpha {\rm d}\Omega_1 {\rm d}\Omega_2} = \frac{\omega}{I}\frac{\partial}{\partial t}\int_0^\infty {\rm d}k_1 \int_0^\infty {\rm d}k_2\, \delta\left(\alpha - \tan^{-1}\left(\frac{k_2}{k_1}\right)\right) \times \left|\sum_{l_1,l_2} (-{\rm i})^{l_1+l_2} {\rm e}^{{\rm i}(\delta_{l_1}+\delta_{l_2})} P^{^1{\rm P}}_{l_1 l_2}(k_1,k_2,t) Y^{^1{\rm P}}_{l_1 l_2}(\hat{k_1},\hat{k_2})\right|^2. \tag{19}$$

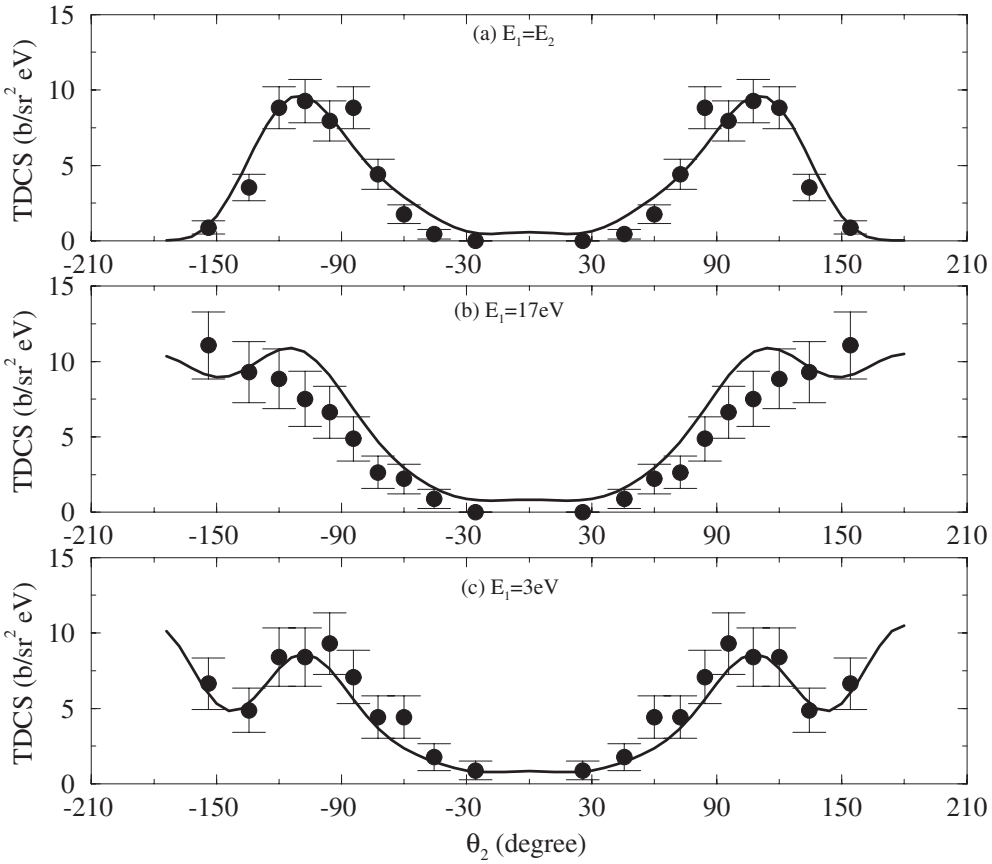

Figure 5. Triple differential cross sections in b/sr^2 eV for helium, as a function of θ_2, for $\theta_1 = 0^\circ$, for three values of the energy of the first ejected electron E_1 as indicated. (1.0b $= 1.0 \times 10^{-24}$ cm^2).

In contrast to equation (15), the sum over $l_1 l_2$ is now inside the square so that the outgoing momentum space wavefunction amplitudes are summed coherently. Since we make use of a projection in equation (9) onto products of radial Coulomb waves, the momentum space amplitudes must also be weighted by the appropriate phases to guarantee projection onto the complex outgoing Coulomb waves. Finally, the orthonormality relations for the coupled momentum spherical harmonics guarantee reduction of equation (19) to equation (15) upon integration over the solid angles for both photoelectrons.

Defining all photoelectron emission angles with respect to the direction of the polarization of the radiation field, triple differential cross sections are presented in figures 4–6 as a function of ejected energies and as a function of θ_1 and θ_2 for co-planar geometry (i.e. $\phi_1 = \phi_2 = 0$). We present Cartesian plots, as opposed to polar plots, to compare as closely as possible with the absolute experimental data of Bräuning *et al* [10]. In figure 4 we present triple differential cross sections at equal energy sharing $E_1 = E_2$ for four values of θ_1 as shown. For all cases over a wide range of θ_2 from $-180 < \theta_2 < 180$ the agreement with experiment is excellent. The peaks mapped out by the experimental data are reproduced by theory in both shape and magnitude; only in one instance does theory give a higher peak than experiment. Only for $\theta_1 = 0^\circ$ do we find any significant cross section in the forward scattering range.

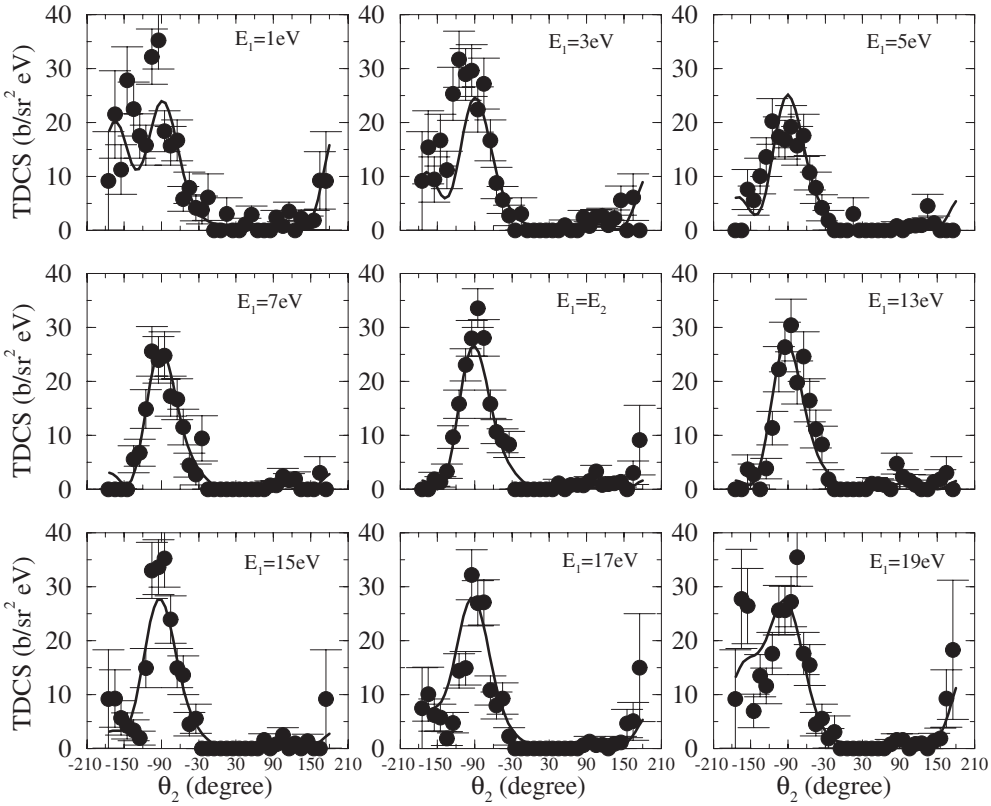

Figure 6. Triple differential cross sections in b/sr^2 eV for helium, as a function of θ_2, for $\theta_1 = 30^\circ$ for various values of the energy of the first ejected electron E_1 as indicated. (1.0b = 1.0×10^{-24} cm^2).

In figure 5 we show the dependence of the triple differential cross section, with fixed $\theta_1 = 0^\circ$, on the energy sharing between the electrons. Again the agreement with the experiment of Bräuning *et al* [10] is excellent in both the shape and magnitude of the triple differential cross section. It is clear that the triple differential cross section is almost zero for small values of θ_2 and reaches a maximum for $|\theta_2| \simeq 100^\circ$. In figure 6 we give a detailed analysis of the triple differential cross section when the energy sharing between the electrons is varied in a consistent manner, at $\theta_1 = 30^\circ$. At all energy sharings the agreement between theory and experiment is still excellent. Apart from the case of most unequal energy sharing ($E_1 = 1$ eV and $E_1 = 19$ eV), where back to back emission becomes enhanced, the triple differential cross section is broadly the same over a wide range of energy sharings.

In summary, the time-dependent close-coupling method has been extended to obtain absolute angular differential cross sections for the double photoionization of helium. Excellent agreement is found between theory and the experimental results of Bräuning *et al* [10] over a wide range of angles and energy sharings of the two outgoing electrons. More work remains to be done on (γ, 2e) processes in systems with simple cores, such as the alkaline earth atoms [20, 21], as well as more challenging open shell core systems [22]. Also, (γ, 2e) processes in molecules, where the process is greatly complicated by the extra vibrational degree of freedom, remains an outstanding challenge. The time-dependent method has also

been used to study (2γ, 2e) processes [23]. It is hoped to extend this method to extract fully differential cross sections in order to obtain maximum information about the outgoing electrons. We also plan to study the (γ, 3e) complete fragmentation of lithium, which has been the subject of much recent work [24, 25]. It is hoped that the application of the time-dependent method can help in the understanding of these highly correlated processes.

We would like to thank R Dörner, H Bräuning and R Wehlitz for communication of their experimental data in numerical form. This work was supported by the US Department of Energy. Computational work was carried out at the National Energy Research Supercomputer Center at the Lawrence Berkeley National Laboratory [26].

References

[1] Proulx D and Shakeshaft R 1993 *Phys. Rev.* A **48** R875–8
[2] Pont M, Shakeshaft R, Maulbetsch F and Briggs J S 1996 *Phys. Rev.* A **53** 3671–4
[3] Kheifets A S and Bray I 1998 *J. Phys. B: At. Mol. Opt. Phys.* **31** L447–53
[4] Kheifets A S and Bray I 2000 *Phys. Rev.* A **62** 065402
[5] Malegat L, Selles P and Kazansky A K 1999 *Phys. Rev.* A **60** 3667–76
[6] Malegat L, Selles P and Kazansky A K 2000 *Phys. Rev. Lett.* **85** 4450–3
[7] Rescigno T N, Baertschy M, Isaacs W A and McCurdy C W 1999 *Science* **286** 2474–9
[8] Bray I 2000 *J. Phys. B: At. Mol. Opt. Phys.* **33** 581–95
[9] Bray I 2000 *Aust. J. Phys.* **53** 355–98
[10] Bräuning H *et al* 1998 *J. Phys. B: At. Mol. Opt. Phys.* **31** 5149–60
[11] Roder J, Rasch J, Jung K, Whelan C T, Ehrhardt H, Allan R J and Walters H R J 1996 *Phys. Rev.* A **53** 225–33
[12] Roder J, Ehrhardt H, Pan C, Starace A F, Bray I and Fursa D V 1997 *Phys. Rev. Lett.* **79** 1666–9
[13] Pindzola M S and Robicheaux F 1998 *Phys. Rev.* A **57** 318–24
Pindzola M S and Robicheaux F 1998 *Phys. Rev.* A **58** 779–80
[14] Levin J C, Armen G B and Sellin I A 1996 *Phys. Rev. Lett.* **76** 1220–3
[15] Dörner R *et al* 1996 *Phys. Rev. Lett.* **76** 2654–7
[16] Samson J A R, Stolte W C, He Z X, Cutler J N, Lu Y and Bartlett R J 1998 *Phys. Rev.* A **57** 1906–11
[17] Pindzola M S and Robicheaux F 2000 *Phys. Rev.* A **61** 052707
[18] Colgan J, Pindzola M S, Mitnik D M and Griffin D C 2001 *Phys. Rev.* A **63** 062709
[19] Wehlitz R, Heiser F, Hemmers O, Langer B, Menzel A and Becker U 1991 *Phys. Rev. Lett.* **67** 3764–7
[20] Beyer H-J, West J B, Ross K J and De Fanis A 2000 *J. Phys. B: At. Mol. Opt. Phys.* **33** L767–71
[21] Malegat L, Citrini F, Selles P and Archirel P 2000 *J. Phys. B: At. Mol. Opt. Phys.* **33** 2409–18
[22] Rioual S, Rouvellou B, Avaldi L, Battera G, Camilloni R, Stefani G and Turri G 2000 *Phys. Rev.* A **61** 044702
[23] Pindzola M S and Robicheaux F 1998 *J. Phys. B: At. Mol. Opt. Phys.* **31** L823–31
[24] Wehlitz R, Pattard T, Huang M-T, Sellin I A, Burgdörfer J and Azuma Y 2000 *Phys. Rev.* A **61** 030704(R)
[25] van der Hart H W and Greene C H 1998 *Phys. Rev. Lett.* **81** 4333–6
[26] It is worth noting that, although these calculations were carried out on NERSC parallel supercomputers, the calculations were sufficiently small that they could have easily been carried out on a workstation. Since only one photon energy was considered, one time-dependent calculation is necessary, from which all triple differential cross sections may be obtained. The implementation of these programs on parallel systems is useful, however, when calculations are necessary over a wide range of energy points or, as in the case of electron scattering, over a large number of partial waves.